Research Article

Journal of Environmental Nanotechnology

Enhanced Room-Temperature Ammonia Sensing Performance of PANI@ZnO/Fe_3O_4Hybrid Nanocomposites Synthesized *via* Chemical Oxidative Polymerization

K. Chandrasekaran[1], G. Chandrasekaran[2], Sathish Kumar Shanmugam[3*], J. Mathan[4], A. V. S. Ram Prasad[5] and S. Mayakannan[6]

[1]Department of Safety and Fire Engineering, K.S.R. College of Engineering, Tiruchengode, Namakkal, TN, India
[2]Department of Mechanical Engineering, Lord Jegannath College of Engineering and Technology, Nagercoil, TN, India
[3]Department of Electrical and Electronics Engineering, M. Kumarasamy College of Engineering, Karur, TN, India
[4]Department of Mechanical Engineering, K S Rangasamy Institute of Technology Thiruchengode, Namakkal, TN, India
[5]Department of Mechanical Engineering, Koneru Lakshmaiah Education Foundation, Guntur, AP, India
[6]Department of Mechanical Engineering, Saveetha School of Engineering, Saveetha Institute of Medical and Technical Sciences, Chennai, TN, India
[6]Department of Mechanical Engineering, School of Engineering and Emerging Technology, Rathinam Global (Deemed to be University), Coimbatore, TN, India

Received: 13.06.2026 Accepted: 15.07.2026 Published: xx.xx.xxxx

*sathishkumar89533@gmail.com

ABSTRACT

Hybrid organic–inorganic nanocomposites have attracted considerable attention owing to their enhanced sensitivity toward oxidizing and reducing gases and their potential for sustainable sensing technologies. In this study, a novel PANI@ZnO/Fe_3O_4 hybrid nanocomposite film was synthesized through chemical oxidative polymerization for high-performance ammonia sensing under ambient conditions. The incorporation of ZnO and Fe_3O_4 nanoparticles into the PANI matrix resulted in measurable changes in the structural, optical, and thermal characteristics of the hybrid nanocomposite. The successful formation of the hybrid nanocomposite was confirmed through X-ray diffraction (XRD), Fourier transform infrared spectroscopy (FTIR), UV–Vis spectroscopy, and thermogravimetric analysis (TGA). The optical band gap decreased from 3.18 eV for pure PANI to 2.79 eV for the PANI@ZnO/Fe_3O_4-5 nanocomposite, indicating improved charge transfer characteristics. Among the fabricated sensors, the PANI@ZnO/Fe_3O_4-5 sensor exhibited the highest sensing response of approximately 215% toward 300 ppm NH_3, with a sensitivity of 0.727 % ppm^{-1} (R^2 = 0.9989) over the investigated concentration range of 50–300 ppm and rapid response and recovery times of about 11 s. The sensor also demonstrated excellent selectivity against interfering gases, including CO, CO_2, H_2S, and ethanol, together with good long-term stability and humidity tolerance. The enhanced sensing performance may be associated with interactions among PANI, ZnO, and Fe_3O_4 nanoparticles and the resulting changes in the sensing behavior toward NH_3. These findings demonstrate the potential of PANI@ZnO/Fe_3O_4 hybrid nanocomposites as sustainable materials for advanced environmental monitoring and room-temperature ammonia sensing applications.

Keywords: Optical band gap; Electrical conductivity; Catalytic activity; Charge transfer; Nano composites.

1. INTRODUCTION

Ammonia (NH_3) is a widely encountered hazardous gas associated with fertilizer production, refrigeration, chemical processing, and environmental emissions. Reliable room-temperature NH_3 detection is particularly attractive because it minimizes heating requirements, reduces energy consumption, and facilitates portable and continuous monitoring (Daramola *et al.* 2025). Despite considerable advances in gas-sensing materials, practical limitations remain in sensitivity, selectivity, humidity tolerance, response–recovery kinetics, long-term stability, and reproducibility (Buledi *et al.* 2023). Room-temperature operation is important because many conventional metal-oxide gas sensors require thermal activation, increasing power consumption and complicating integration into portable sensing platforms. Current NH_3 sensors also exhibit trade-offs among low-concentration sensitivity, gas selectivity, humidity resistance, response–recovery speed, and operational stability. Consequently, development of hybrid sensing materials capable of efficient NH_3 adsorption and charge modulation under ambient conditions remains important. Contemporary gas sensing research is primarily directed toward nanoscale metal oxide-based sensors, metal–polymer composite systems, and biosensors that offer improved analyte selectivity and detection performance

(Gunasekaran *et al.* 2025). Despite remarkable progress, challenges related to stability, reproducibility, and large-scale implementation remain significant concerns in practical applications (Murugan *et al.* 2025). Iron oxide-based nanomaterials have emerged as promising sensing platforms owing to their catalytic activity, biocompatibility, and ease of functionalization. A peroxidase-simulating FeOx/C nanozyme prepared through electrospinning and subsequent calcination demonstrated excellent catalytic activity, enabling highly sensitive colorimetric detection of ascorbic acid under optimized synthesis conditions (Liu *et al.* 2022). Similarly, surface-functionalized Fe_3O_4 nanoparticles integrated with electrochemical platforms exhibited excellent analytical performance, achieving low detection limits and high selectivity for biomolecule monitoring (Niaz *et al.* 2025). Magnetic nanohybrid systems have also been successfully incorporated into portable sensing devices, highlighting their suitability for rapid and on-site detection applications (Pakapongpan *et al.* 2022). Fluorescent iron oxide nanoparticle-based sensors have shown significant potential for environmental monitoring. Functionalization with fluorophore molecules enabled rapid and selective detection of toxic heavy metal ions through fluorescence quenching mechanisms, achieving excellent discrimination against interfering ions in aqueous systems (Bilgic and Cimen, 2020). In another approach, pyrene-modified iron oxide nanoparticles exhibited efficient "turn-off" fluorescence behavior for mercury ion detection, providing nanomolar-level sensitivity suitable for environmental analysis (Tümay et al., 2021).

The incorporation of iron oxide nanoparticles into conductive polymer matrices has further expanded their sensing capabilities. Nanocomposite electrodes composed of polyaniline (PANI), graphene derivatives, and iron oxide nanoparticles exhibited enhanced electron transfer kinetics and catalytic activity, resulting in highly sensitive non-enzymatic glucose detection over broad concentration ranges (Ghaffarirad *et al.* 2024). Likewise, microbial fuel cell-based biosensors modified with iron oxide nanoparticles and conductive polymers enabled rapid biochemical oxygen demand (BOD) monitoring with excellent analytical accuracy and short response times (Yang *et al.* 2025). Beyond sensing applications, iron oxide nanocomposites have demonstrated multifunctionality in energy storage systems. Electrochemically synthesized PANI/iron oxide films exhibited enhanced magnetic properties, while nanocomposite electrodes incorporating Fe_3O_4 and graphitic carbon nitride delivered high capacitance and long-term cycling stability, indicating strong synergistic electrochemical behavior (Al-Gharram *et al.* 2024), (Yang *et al.* 2020). Furthermore, silver-doped Fe_2O_3 nanoparticles and other modified iron oxide systems have shown promising electrochemical characteristics for both sensing and energy storage applications (Velayudham and Natarajan, 2025). Green synthesis approaches have increasingly been employed to produce environmentally sustainable nanomaterials with excellent functional performance. Plant-mediated iron oxide nanoparticles have been successfully utilized for sensitive electrochemical sensing of target analytes, demonstrating low detection limits and broad linear response ranges (Hasan *et al.* 2021). Biosynthesized iron oxide-gold nanocomposites have also been explored for pathogen detection, providing cost-effective and efficient diagnostic platforms (Shanavash *et al.* 2026).

Recent investigations have highlighted the biomedical relevance of iron oxide nanoparticles. Microwave-assisted synthesized Fe_3O_4 nanoparticles possessing high saturation magnetization and controlled crystallite size have been proposed for magnetic resonance imaging, targeted drug delivery, hyperthermia treatment, and biosensing applications (Singh *et al.* 2025). Drug-loaded Fe_3O_4-based nanocarriers functionalized with amino acid ligands demonstrated controlled pH-responsive drug release and significant anticancer activity against melanoma cell lines, emphasizing their therapeutic potential (Toderascu *et al.* 2023). ZnO-based nanocomposites combined with conductive polymers have also gained considerable attention for sensor development. Thulium-doped ZnO/PANI nanocomposites exhibited excellent electrochemical performance for dopamine detection, providing high sensitivity and low detection limits (Yıldız *et al.* 2024). Similarly, PANI/ZnO nanocomposite films have been employed in conductometric immunosensors for pathogen detection and voltammetric sensors for preservative monitoring, demonstrating broad analytical applicability (Mutlaq *et al.* 2021), (Manasa *et al.* 2019). Optimized PANI/ZnO systems have additionally shown effective non-enzymatic cholesterol sensing capabilities with satisfactory sensitivity and linear response characteristics (Murugesan *et al.* 2024).

Flexible and wearable sensing devices have further benefited from ZnO-polymer nanocomposite architectures. Electrospun ZnO/PANI-based humidity sensors demonstrated rapid response behavior across a wide humidity range and were successfully utilized for real-time respiratory monitoring applications (Yan *et al.* 2023). Likewise, chitin nanowhisker/ZnO/PANI nanocomposites enabled room-temperature ethanol sensing with low detection limits, highlighting their potential for wearable electronics and Internet of Things (IoT) technologies (Andre *et al.* 2020). Advanced hybrid nanostructures integrating noble metals and magnetic nanoparticles have also been explored for biosensing applications. Hollow Pt–Fe_3O_4@C nanocomposites exhibited excellent catalytic activity and biocompatibility, enabling sensitive sarcosine detection for prostate cancer screening (Yang *et al.* 2019). Furthermore, carbon-supported Fe_2O_3 nanocomposites functionalized with cysteine demonstrated ultratrace detection of toxic heavy metal ions owing to their strong

adsorption affinity and enhanced electrochemical activity (Basha *et al.* 2025). In addition to electrochemical sensing, iron oxide nanomaterials have shown excellent gas sensing capabilities. Hydrothermally synthesized α-Fe_2O_3 nanoparticles possessing high surface area and favorable porous morphology demonstrated superior ammonia sensing performance at room temperature, accompanied by rapid response and recovery characteristics indicating their suitability for practical gas monitoring applications (Rajyashree *et al.* 2023).

The novelty of this study lies in the development and systematic evaluation of PANI@ZnO/Fe_3O_4 ternary nanocomposite films for room-temperature NH_3 sensing. In contrast to conventional PANI/metal-oxide binary systems, the present work combines conductive PANI with ZnO and Fe_3O_4 to exploit their complementary contributions to NH_3 adsorption, interfacial charge modulation, and resistance-based sensing. The controlled variation of ZnO/Fe_3O_4 loading enables direct assessment of composition-dependent effects on sensing response, response–recovery kinetics, selectivity, long-term stability, and humidity tolerance. The ternary architecture is intended to provide a synergistic sensing environment through PANI protonation–deprotonation behavior together with additional adsorption and interfacial sites introduced by the metal oxides. Thus, the study contributes a comparatively underexplored PANI/ZnO/Fe_3O_4 sensing platform for low-power, ambient-temperature ammonia detection and environmental monitoring.

2. MATERIALS AND METHODOLOGY

2.1 Materials

The substances and materials utilized in the experimental study are procured from Star Scientific Enterprises, Erode, Tamil Nadu, India, and are delineated in Table 1. All reagents were employed as received without any additional purification. Double-deionized water were uniformly employed for formulation of all experimental solutions during the study.

Table 1. Chemicals utilized in the synthesis process

S. No.	Chemical	Formula	Molecular Weight ($g\ mol^{-1}$)
1	Polyaniline	C_6H_7N	93.13
2	Ammonium persulfate (APS)	$(NH_4)_2\ S_2O$	228.20
3	Hydrochloric acid	HCl	36.46
4	Zinc oxide	ZnO	81.38
5	Iron oxide	Fe_3O_4	231.53

2.2 Synthesis of Polyaniline

Polyaniline was created by chemical oxidative polymerization of aniline in an acidic environment. The aniline monomer was initially dissolved in 1 M hydrochloric acid (HCl) with continuous magnetic stirring to produce an anilinium chloride solution. Ammonium persulfate (APS) was independently dissolved in 1 M HCl and utilized as an oxidizing agent.

An APS solution was introduced dropwise into the aniline solution while maintaining steady stirring at a temperature of 0–5 °C. The reaction mixture was agitated constantly for 4–6 hours and subsequently allowed to stand undisturbed for 1 day to ensure full polymerization. A dark green precipitate of PANI emeraldine salt was obtained using vacuum filtration and subsequently washed multiple times with deionized water, ethanol, and weak HCl to eliminate unreacted monomer, oligomers, and residual oxidant. The resultant PANI powder was dried in a hot-air oven at 50–60 °C for 1 day until a constant weight was attained (Tamilarasi *et al.* 2026).

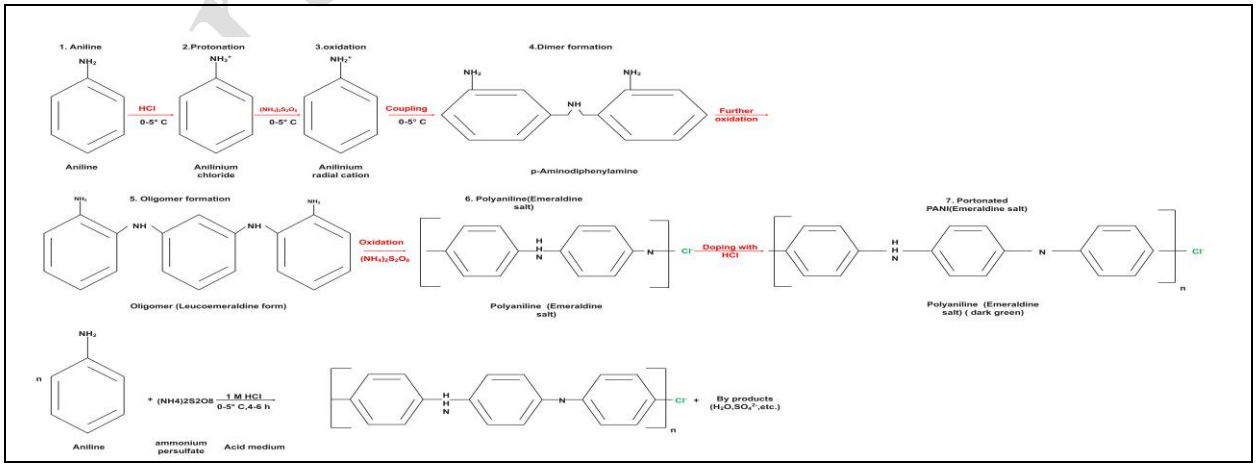

Fig. 1: Acid-mediated synthesis of polyaniline

2.3 Preparation of PANI@ZnO/Fe_3O_4 Hybrid Nanocomposite

Figure 2 illustrates the in situ chemical oxidative polymerization process employed for the synthesis of the PANI@ZnO/Fe_3O_4 hybrid nanocomposite. Initially, 1 M aniline monomer was solubilized in a 0.15 M hydrochloric acid solution under continuous magnetic stirring at 500 rpm to obtain a homogeneous anilinium chloride solution. Independently, precursor solutions including Zinc nitrate [$Zn(NO_3)_2 \cdot 6H_2O$] and Magnetite (Fe_3O_4) nanoparticles were formulated in 10 mL of distilled water and ultrasonicated at 40 kHz and 100 W for 30 min to obtain stable suspensions.

The metal precursor solutions were subsequently incorporated into the aniline solution in specified ratios and continually agitated to create a uniform reaction mixture. APS dissolved in 0.15 M HCl was gradually added as the oxidizing agent under ice-bath conditions (0–5 °C). The total reaction volume was adjusted to approximately 100 mL using distilled water, and oxidative polymerization was continued for 6 h under continuous stirring at 500 rpm. The resulting dark-green precipitate was recovered by vacuum filtration using Whatman No. 1 filter paper and washed three times with deionized water followed by ethanol to remove residual reactants and impurities.

The recovered PANI@ZnO/Fe_3O_4 hybrid nanocomposite was dried in a hot-air oven under atmospheric air at 60 °C for 24 h. The ZnO/Fe_3O_4 loadings were systematically varied from 0.10/0.05 to 1.00/0.40 g while maintaining 0.6 g PANI to investigate the effect of metal oxide loading on the properties and NH_3 sensing performance of the hybrid nanocomposites.

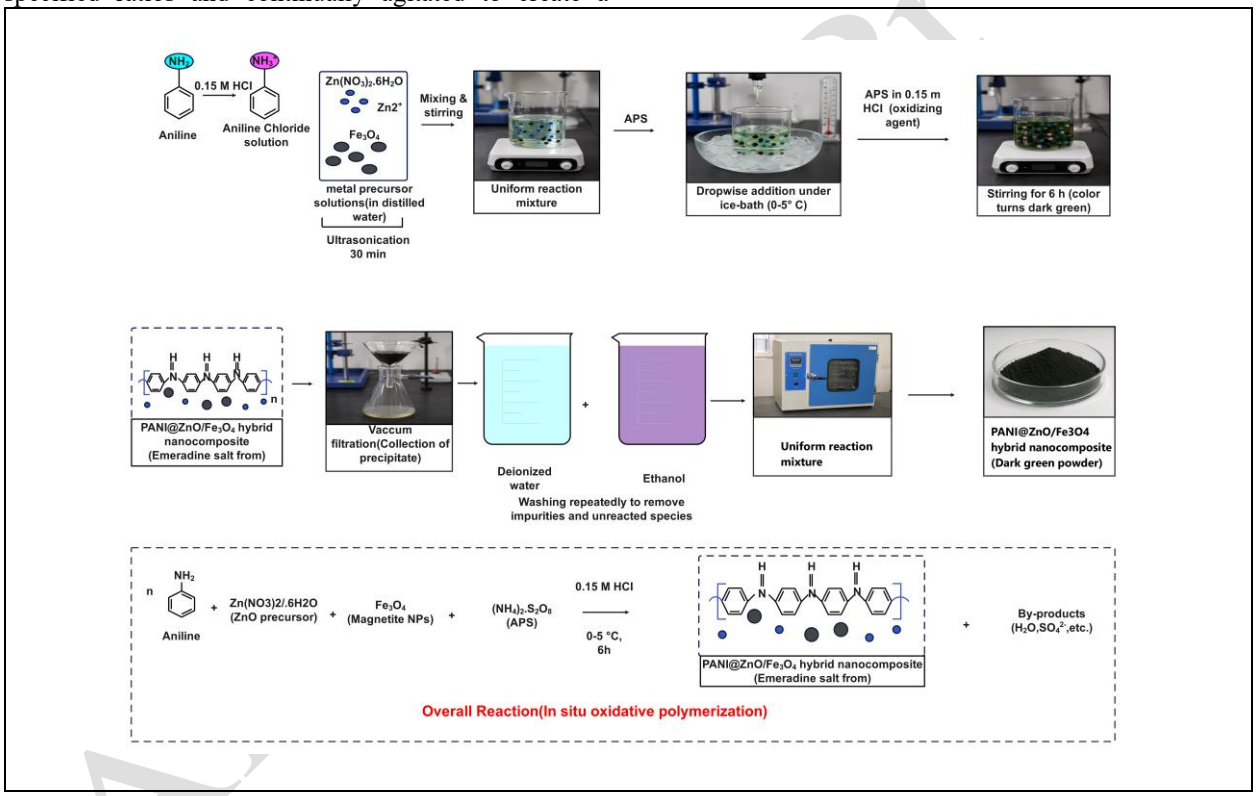

Fig. 2: Schematic illustration of the in-situ chemical oxidative polymerization process for the preparation of PANI@ZnO/Fe_3O_4 hybrid nanocomposites

PANI@ZnO/Fe_3O_4 hybrid nanocomposites were manufactured utilizing varying concentrations of Zinc oxide and Fe_3O_4 nanoparticles. The ZnO/Fe_3O_4 filler contents were changed at 0.10/0.05 g, 0.25/0.10 g, 0.50/0.20 g, 0.75/0.30 g, and 1.00/0.40 g, with the resulting samples denoted PANI@ZnO/Fe_3O_4-1, PANI@ZnO/Fe_3O_4-2, PANI@ZnO/Fe_3O_4-3, PANI@ZnO/Fe_3O_4-4, and PANI@ZnO/Fe_3O_4-5 as depicted at Table 2.

Table 2. Composition of PANI@ZnO/Fe_3O_4 hybrid nanocomposites

Sample Designation	PANI (g)	Fe_3O_4 Loading (g)	ZnO Loading (g)
PANI	0.60	0	0
PANI@ZnO/Fe_3O_4-1	0.60	0.05	0.10

PANI@ZnO/Fe₃O₄-2	0.60	0.10	0.25
PANI@ZnO/Fe₃O₄-3	0.60	0.20	0.50
PANI@ZnO/Fe₃O₄-4	0.60	0.30	0.75
PANI@ZnO/Fe₃O₄-5	0.60	0.40	1.00

2.4 Mechanism of Stabilization in PANI@ZnO/Fe_3O_4 Hybrid System

The imine and amine functional groups on the PANI backbone engage robustly with ZnO and Fe_3O_4 nanoparticles via coordination bonding, facilitating the uniform stability and dispersion of metal oxide particles inside the polymer matrix. In the production of hybrid nanocomposites, interfacial redox interactions facilitate the efficient integration of ZnO and Fe_3O_4 nanoparticles into the conductive PANI matrix without the need for supplementary stabilizing chemicals. The superior electrical conductivity and catalytic properties of ZnO and Fe_3O_4 markedly improve the charge transfer dynamics and sensing efficacy of the PANI matrix. This synergistic interaction enhances the gas sensing capabilities and overall functional attributes of the produced nanocomposite. Figure 3 demonstrates that, PANI chains with amine functionalities efficiently prevent the aggregation of ZnO/Fe_3O_4 nanoparticles and ensure a steady distribution of nanoparticles within the matrix.

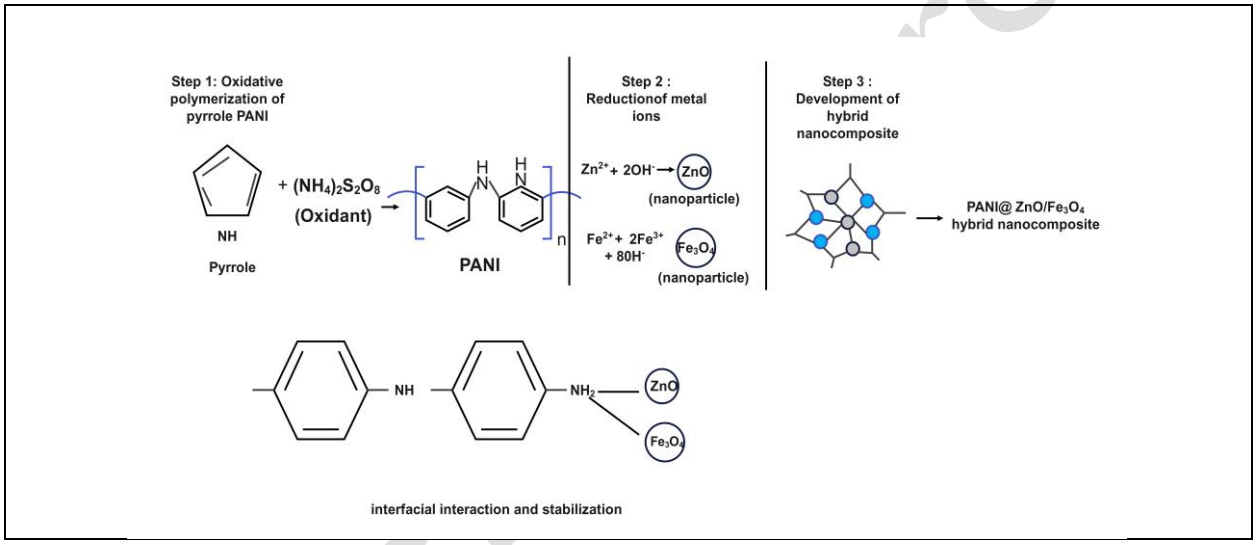

Fig. 3: Stabilization of PANI@ ZnO /Fe_3O_4 hybrid nanocomposite

The comprehensive reaction can be encapsulated as follows:

Oxidative polymerization of Polyaniline

$$nC_6H_5NH_2 + (NH_4)_2S_2O_8 \rightarrow (C_6H_4NH)_n + 2NH_4HSO_4 \ldots (1)$$

Incorporation of ZnO and Fe_3O_4 nanoparticles into PANI matrix:

$$\text{PANI} + \text{ZnO NPs} + Fe_3O_4\ \text{NPs} \rightarrow \text{PANI@ZnO/}Fe_3O_4\ \text{hybrid nanocomposite} \quad \ldots (2)$$

During oxidative polymerization, ZnO and Fe_3O_4 nanoparticles were incorporated into the growing PANI matrix to form the PANI@ZnO/Fe_3O_4 hybrid nanocomposite. This representation denotes nanoparticle incorporation rather than a reduction reaction.

The incorporation of ZnO and Fe_3O_4 nanoparticles into the PANI matrix may promote interfacial interactions between the polymer and metal oxide components. This interpretation is supported by the observed FTIR spectral changes, including the shift in the N–H stretching band and the characteristic Fe–O and Zn–O vibrations. However, the precise interfacial stabilization mechanism cannot be conclusively established from FTIR analysis alone.

2.5 Preparation of PANI Film

Pure Polyaniline (PANI) was dispersed in N-methyl-2-pyrrolidone (NMP) to achieve a homogeneous viscous solution, attributed to robust intermolecular interactions and elongated conjugated polymer chains of PANI. NMP is a highly polar aprotic solvent that efficiently dissolves conductive polymers while maintaining the structural integrity of the PANI backbone. The resultant viscous properties promote the creation of homogeneous thin films, which is beneficial for gas sensing applications. The PANI solution was applied to a silicon substrate by the spin-coating technique at 1500 rpm for 20 seconds to achieve a

uniform sensing layer. Electrical connections were subsequently formed utilizing zinc paste on the coated PANI film, with both the electrode track width and inter-electrode spacing consistently set at 1 mm.

2.6 Preparation of PANI@ ZnO /Fe_3O_4 Film

To formulate the sensing solution, 2 mg of synthesized PANI/Fe_3O_4/ZnO hybrid nanocomposite was dispersed in 0.1 M polyvinyl pyrrolidone (PVP) while continuously stirring to achieve a stable coated suspension. The resultant slurry was applied to a silicon substrate via the spin-coating method at 1500 rpm for 10 seconds to create a homogeneous sensor film. Zinc paste was next utilized to create electrical contacts on the produced conductive film, as shown in Figure 4.

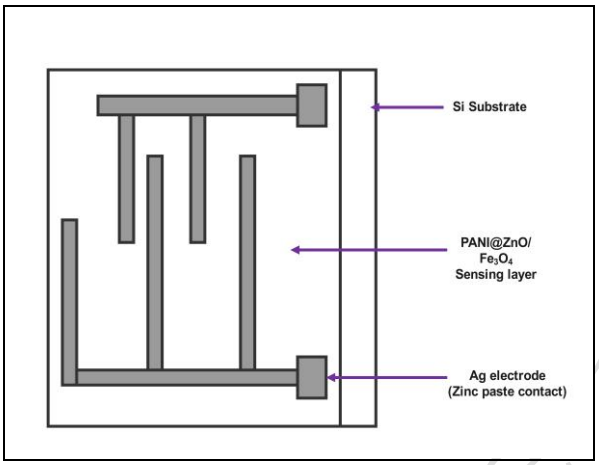

Fig. 4: Fabricated PANI@ZnO nanocomposite film

3. RESULTS AND DISCUSSION

3.1 X-ray Diffraction (XRD)

Figure 5 depicts the XRD of pure PANI and PANI@ZnO/Fe_3O_4 hybrid nanocomposites with different amounts of ZnO and Fe_3O_4 nanoparticles. The extensive diffraction peak located at 25.2° in Figure 5(a) validates the partly amorphous nature of PANI. The hybrid nanocomposites have numerous pronounced and distinct diffraction peaks, signifying the crystalline properties of ZnO and Fe_3O_4 nanoparticles incorporated inside the polymer matrix. The diffraction peaks at 31.8°, 34.4°, 36.3°, and 47.5° are assigned to (100), (002), (101), and (102) planes of hexagonal ZnO (JCPDS/PDF No. 36-1451), whereas the peaks at 30.2°, 35.5°, 43.2°, 53.5°, 57.1°, and 62.7° correspond to (220), (311), (400), (422), (511), and (440) planes of cubic Fe_3O_4 (JCPDS/PDF No. 19-0629). Table 3 illustrates the substantial impact of ZnO and Fe_3O_4 concentration on nucleation behavior and crystalline development in the nanocomposite system, as evidenced by the variance in crystallite size. The observed diffraction changes suggest that ZnO and Fe_3O_4 incorporation influences the structural ordering of the PANI matrix, while the characteristic oxide reflections confirm the retention of the crystalline phases in the hybrid nanocomposites.

Table 3. XRD-derived structural parameters of PANI@ZnO/Fe_3O_4 hybrid nanocomposites

Sample Designation	2θ of Intense Peak (°)		FWHM of Intense Peak (°)		Crystallite Size (nm)		*d*-spacing (nm)		Lattice Parameter (Å)		Microstrain (ε)		Dislocation Density	
	ZnO	Fe_3O_4	ZnO	Fe_3O_4	ZnO	Fe_3O_4	ZnO	Fe_3O_4	ZnO	Fe_3O_4	ZnO	Fe_3O_4	ZnO	Fe_3O_4
PANI@ZnO/Fe_3O_4-1	36.28	35.48	0.42	0.51	20.4	16.8	0.2474	0.2528	3.249	8.392	5.67	7.12	2.40	3.54
PANI@ZnO/Fe_3O_4-2	36.30	35.50	0.39	0.48	22.1	18.0	0.2473	0.2527	3.250	8.394	5.25	6.70	2.05	3.09
PANI@ZnO/Fe_3O_4-3	36.32	35.53	0.35	0.44	24.6	20.1	0.2472	0.2525	3.251	8.397	4.72	6.11	1.65	2.47
PANI@ZnO/Fe_3O_4-4	36.34	35.56	0.31	0.40	27.8	22.3	0.2471	0.2523	3.252	8.401	4.18	5.56	1.29	2.01
PANI@ZnO/Fe_3O_4-5	36.37	35.60	0.28	0.36	30.8	24.9	0.2469	0.2521	3.254	8.405	3.78	5.02	1.05	1.61

The small size of the crystallites in the PANI matrix was attributed to the increased nucleation effect of the uniformly distributed nanoparticles at lower loadings of ZnO and Fe_3O_4, leading to preferential grain growth and the formation of smaller crystallites in the PANI matrix. Conversely, an increase in the concentration of the nanoparticles resulted in the growth of crystallite size mainly as a result of the nanoparticles' agglomeration and the formation of larger crystalline domains. This crystallite size difference is the result of combined

nucleation effects, interactions between particles, and crystal growth mechanisms in the hybrid nanocomposite system. The mean crystallite size was determined using Scherrer's equation (equation (3)):

$$D = \frac{k\lambda}{\beta \mathrm{Cos}\theta} \qquad \ldots (3)$$

The λ = 0.154 nm represents the Cu-Kα X-ray wavelength, θ shows the Bragg diffraction angle, β represents the full width at half maximum of the diffraction peak, and D represents the average crystallite size in Scherrer's equation. The calculated crystallite size values are given in Table 3. The incorporation of ZnO and Fe_3O_4 nanoparticles significantly influenced the crystallinity and lattice structure of the PANI hybrid nanocomposites. As shown in Figure 5(b), the characteristic diffraction peaks are observed around 30.2°, 31.8°, 34.4°, 35.5°, and 36.3°, corresponding to Fe_3O_4 (220), ZnO (100), ZnO (002), Fe_3O_4 (311), and ZnO (101), respectively. Slight variations in the diffraction-peak positions were observed with increasing ZnO/Fe_3O_4 loading, suggesting composition-dependent changes in the structural characteristics of the hybrid nanocomposites. The Williamson–Hall (W–H) method was further employed to evaluate the contributions of crystallite size and microstrain to XRD peak broadening using $\beta\cos\theta = k\lambda/D + 4\varepsilon\sin\theta$. The linear plots of βcosθ against 4sinθ for PANI@ZnO/Fe_3O_4-1 to PANI@ZnO/Fe_3O_4-5 are presented in Fig. 5(c–g). The slope of the linear fit represents the microstrain (ε), while the intercept corresponds to kλ/D. The calculated microstrain progressively decreased from 0.0072 to 0.0040 with increasing ZnO/Fe_3O_4 loading, whereas the corresponding W–H crystallite size increased from approximately 49.5 to 77.0 nm. This trend indicates a reduction in average lattice microstrain together with the development of larger coherent crystalline domains at higher nanoparticle loadings.

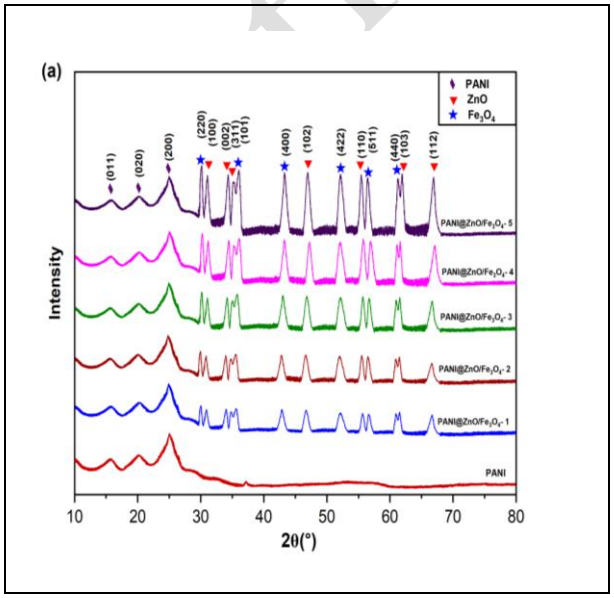

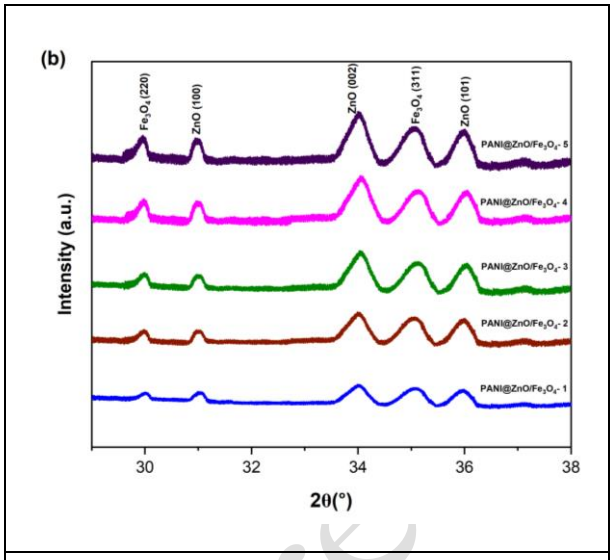

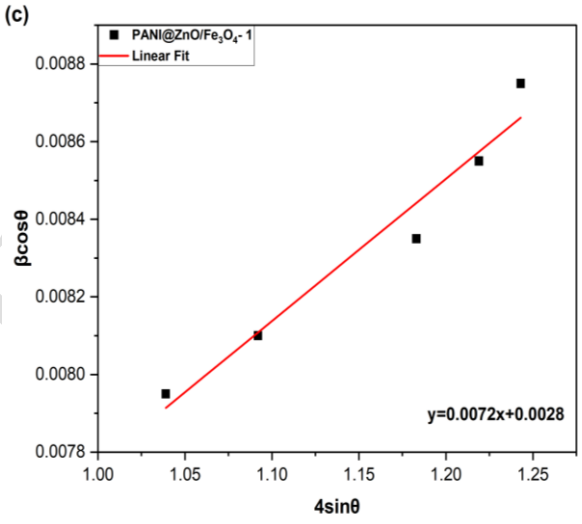

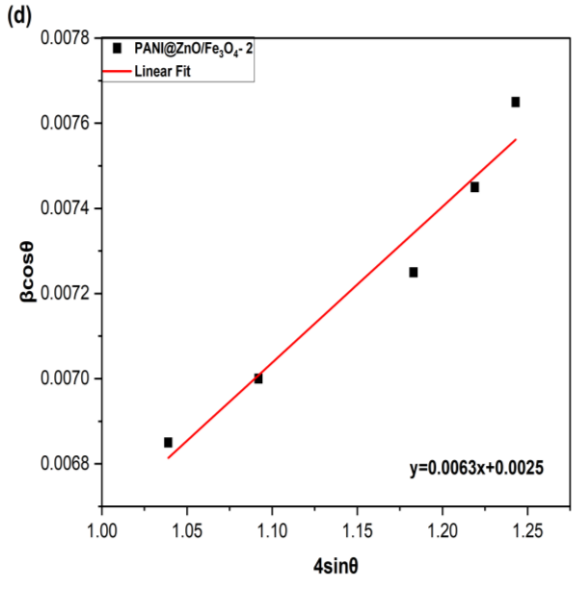

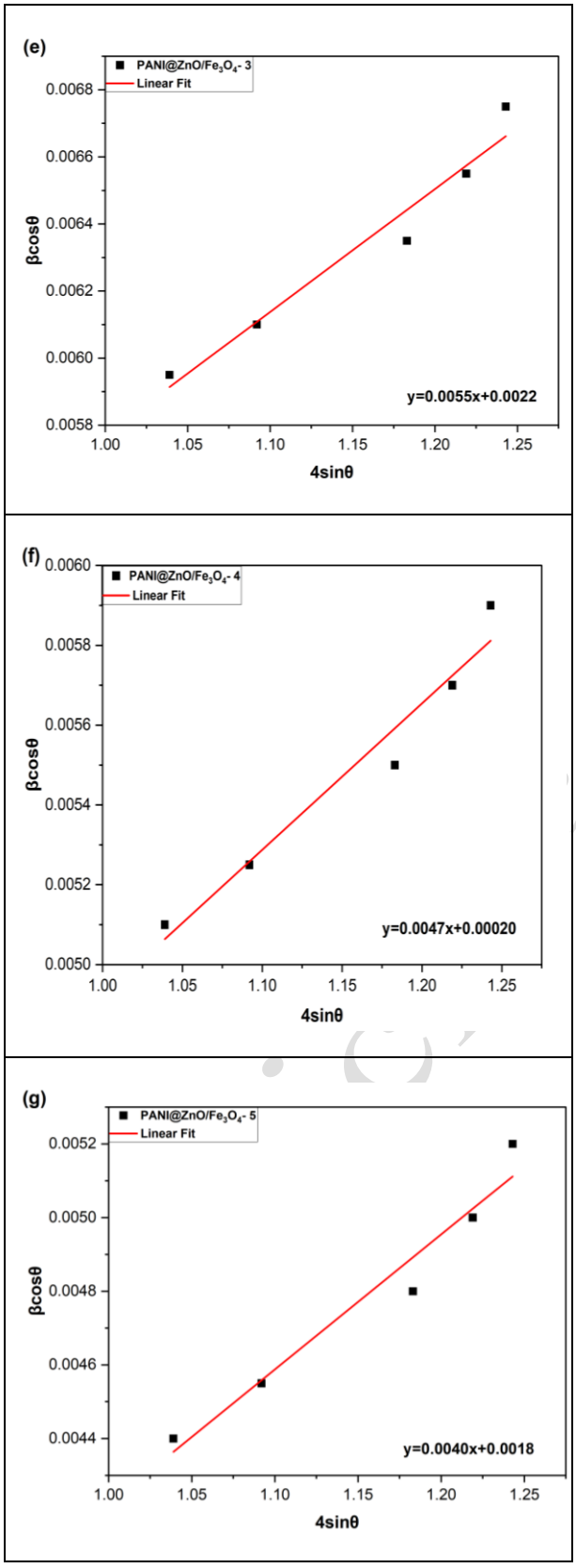

Fig. 5: (a) XRD spectra of PANI@ZnO/Fe_3O_4 nanocomposites; (b) enlarged XRD patterns showing characteristic ZnO and Fe_3O_4 peaks; (c–g) Williamson–Hall plots of ZnO and Fe_3O_4

3.2 FT-IR Study

FTIR analysis was used to verify the successful integration of ZnO and Fe_3O_4 nanoparticles into the PANI matrix and the resulting changes in the functional groups and intermolecular forces of the hybrid nanocomposite. The changes in the structure have a great effect on the developed material's sensing and electrical properties. Fig. 6 shows the FTIR spectra of the generated nanocomposites. The absorption fringes in the range of 1556 cm^{-1} are considered an important band that is associated with the stretching vibration of a quinoid ring structure in the PANI backbone, confirming the formation of the conductive backbone.

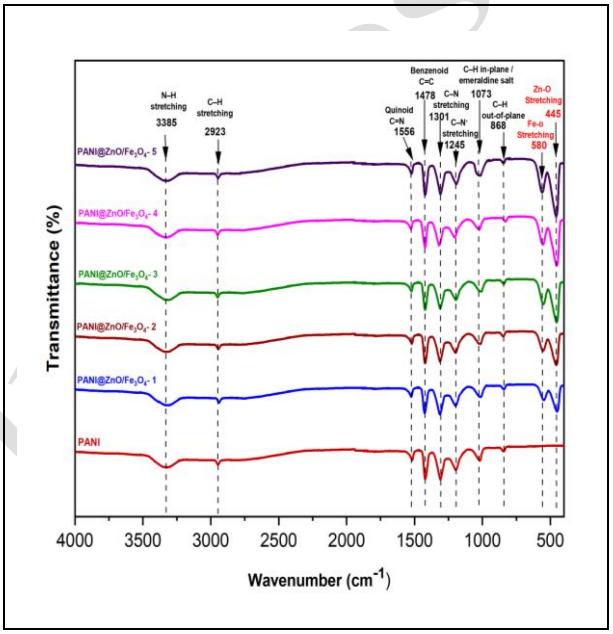

Fig. 6: FTIR spectra of PANI@ZnO/Fe_3O_4 nanocomposites

The absorption band at around 1301 cm^{-1} is ascribed to C–N stretching vibrations, hence affirming the existence of nitrogen-containing functional groups inside the PANI backbone. The unique peaks observed at 868 cm^{-1} and 1073 cm^{-1} were assigned to aromatic C–H out-of-plane deformation and C–H in-plane bending vibrations, respectively. With the incorporation of Fe_3O_4 and ZnO nanoparticles, the broad band around 3385 cm^{-1} shifted to approximately 3388 cm^{-1}, suggesting changes in the local chemical environment of the N–H groups following incorporation of the metal oxide nanoparticles. Additional characteristic absorption bands appeared at 580 cm^{-1} and 445 cm^{-1}, corresponding to Fe–O and Zn–O stretching vibrations, respectively, confirming the successful incorporation of Fe_3O_4 and ZnO nanoparticles into the PANI matrix. This broad spectral range from 1478 to 1556 cm^{-1} suggests the presence of conjugation in PANI and might suggest some electronic interaction with the included nanoparticles. The shift in characteristic wavenumbers of the bands to higher frequencies in the FTIR spectra suggests that the bonding

strength in the PANI framework and the chemical environment of the respective components are changed upon the inclusion of ZnO/Fe_3O_4 in the PANI matrix. These spectral changes suggest modification of the local chemical environment of PANI and possible interfacial interactions between the polymer matrix and the incorporated metal oxide nanoparticles. Prior investigations have shown that Fourier Transform Infrared (FTIR) spectroscopy was employed to verify the successful formation of the Fe_3O_4/Borophene core–shell nanostructure and to identify the characteristic functional groups associated with both Fe_3O_4 nanoparticles and borophene nanosheets. The FTIR spectra confirmed the presence of Fe–O bonding along with boron-related vibrational modes, indicating effective encapsulation of Fe_3O_4 within the borophene shell (Pandey *et al.* 2025).

3.3 UV–Vis Analysis and Band Gap Estimation

The absorption spectrum of pure PANI is shown in Figure 7(a), which shows that a significant absorption peak was observed around 250 nm, corresponding to the π–π electronic transition of the conjugated PANI backbone. Another characteristic absorption peak appears at 330 nm, corresponding to the π–π* transition associated with the quinoid structure, while a broad polaronic absorption band is observed around 615 nm. The presence of ZnO and Fe_3O_4 nanoparticles within the PANI matrix was also confirmed by plotting the UV–Vis spectra of PANI@ZnO/Fe_3O_4 hybrid nanocomposites, as shown in Fig. 7(b). The absorbance bands obtained for the nanocomposite samples were found to be different from 204–208 nm, confirming successful dispersion of Fe_3O_4 and ZnO nanoparticles within polymer matrix. The quinoid/benzenoid transition bands were observed at 330, 332, 334, 336, and 338 nm, while the polaron–π* transition bands appeared at 602, 605, 608, 612, and 615 nm for PANI@ZnO/Fe_3O_4-1 to PANI@ZnO/Fe_3O_4-5, respectively. The hybrid nanocomposites exhibited composition-dependent changes in absorption intensity following the incorporation of ZnO and Fe_3O_4 nanoparticles. The progressive shift in the absorption bands with increasing nanoparticle loading suggests modification of the optical and electronic environment of the PANI-based hybrid system. The progressive decrease in optical band gap indicates composition-dependent modification of the electronic structure of the PANI-based hybrid system. This trend is consistent with the observed variation in NH_3 sensing response, although direct electrical measurements would be required to confirm the associated charge-transport mechanism. The UV–Vis results confirmed the successful incorporation of Cu and Au nanoparticles into the iron oxide matrix, leading to modified electronic properties that contributed to enhanced NO_2 gas sensing performance. The improved optical response was attributed to the synergistic interaction between the dopant nanoparticles and the iron oxide host material (Mahmood *et al.* 2024).

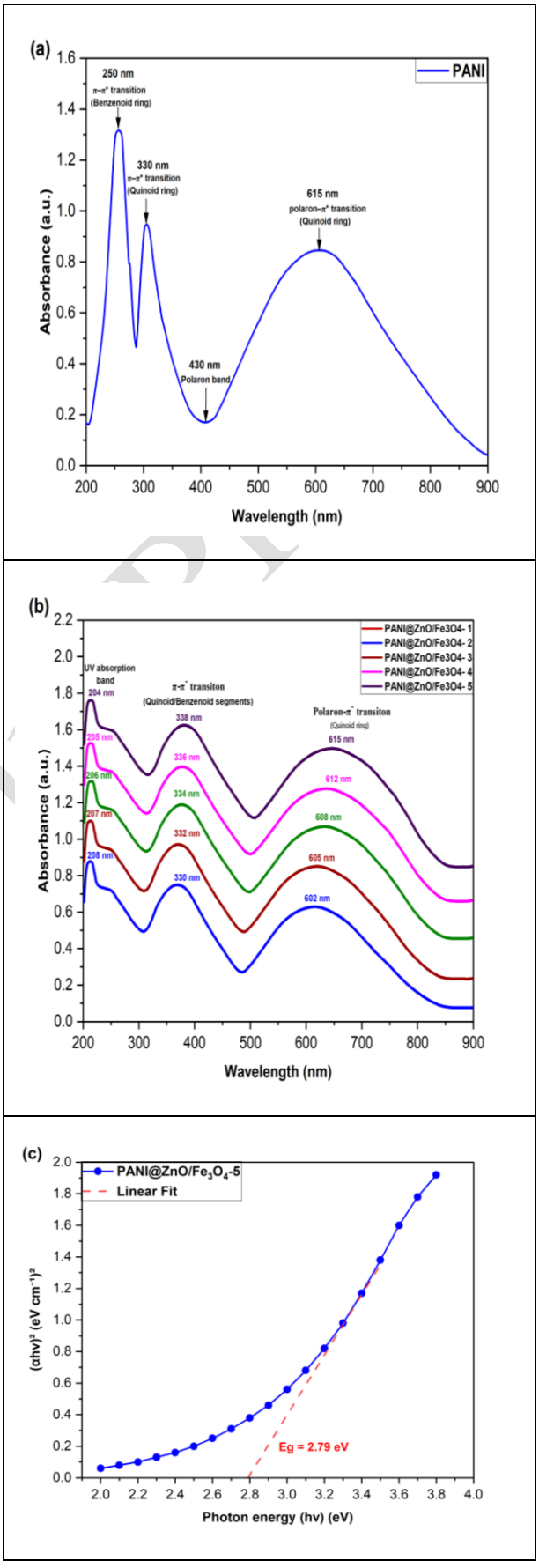

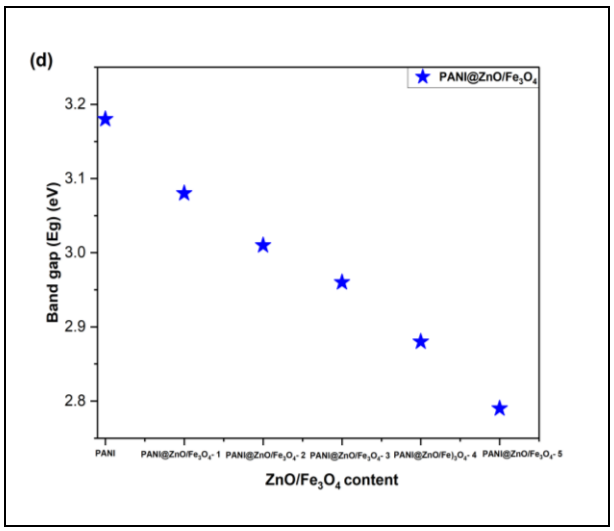

Fig. 7: (a) Optical absorption spectrum of PANI (b) UV–Vis spectra of hybrid nanocomposites; (c) - (d) Band gap analysis of PANI and hybrid nanocomposites

The optical band gap of the manufactured specimens was estimated by Tauc's relation and the direct allowed transition model. Band gap energies were ascertained by extrapolating the linear segment of the $(\alpha h\nu)^2$ versus photon energy graph to the point where $(\alpha h\nu)^2$ equals zero. Figure 7(c and d) demonstrates that, the computed band gap values were around 3.18 eV for PANI, 3.08 eV for PANI@ZnO/Fe_3O_4-1, 3.01 eV for PANI@ZnO/Fe_3O_4-2, 2.96 eV for PANI@ZnO/Fe_3O_4-3, 2.88 eV for PANI@ZnO/Fe_3O_4-4 and 2.79 eV for PANI@ZnO/Fe_3O_4-5 hybrid nanocomposites. The optical band gap progressively decreased from 3.18 eV for pure PANI to 2.79 eV for PANI@ZnO/Fe_3O_4-5 with increasing ZnO/Fe_3O_4 loading. This consistent decrease indicates a composition-dependent modification of the optical and electronic characteristics of the PANI-based hybrid system. The observed trend suggests that the incorporation of ZnO and Fe_3O_4 nanoparticles modifies the local electronic environment of the PANI matrix; however, further direct electronic characterization would be required to establish the underlying mechanism.

3.4 TG–DTA Analysis of Synthesized Materials

Thermogravimetric evaluation was conducted to assess thermal degradation characteristics and stability of produced PANI and PANI@ZnO/Fe_3O_4 hybrid nanocomposites, as depicted in Fig. 8. The TG analysis provides valuable information on the mass variation related to adsorption/desorption processes within the sensing material. Weight changes in the sample during heating might be due to the release of physically adsorbed gases, moisture, or volatile components from the nanocomposite surface. The thermal properties of the produced samples were examined by simultaneous TGA and DTA measurements in a dynamic nitrogen environment with a heating rate of 10 °C min^{-1}.

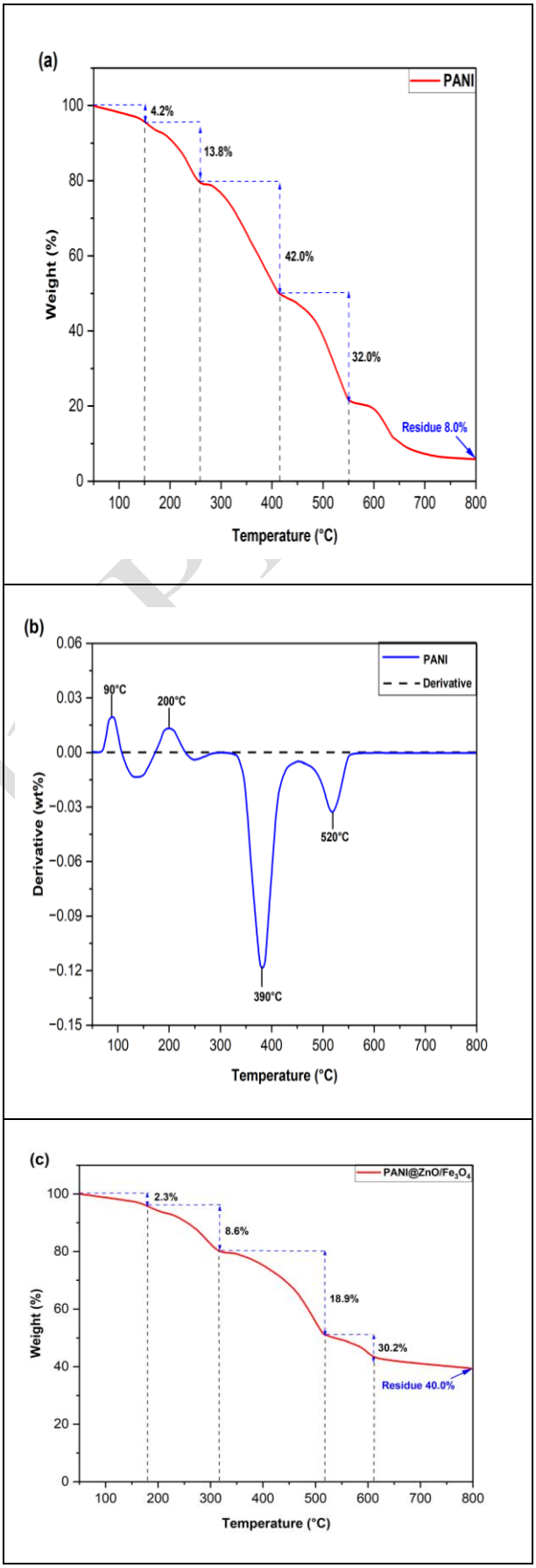

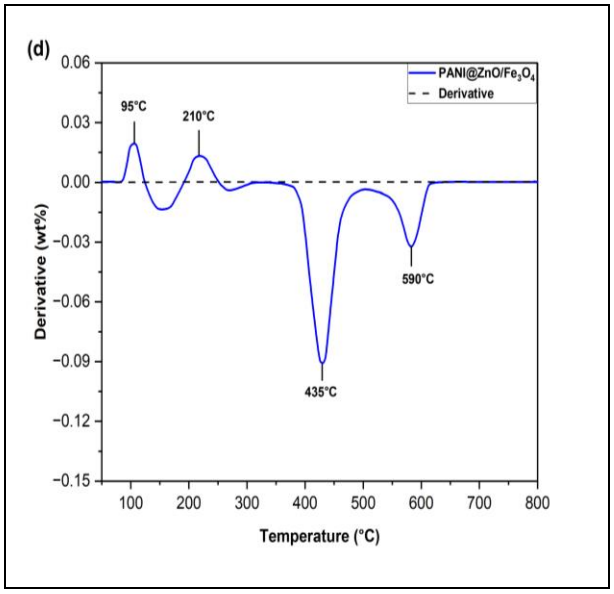

Fig. 8: (a) and (b) TG–DTA curves of PANI (c) and (d) TG–DTA curves of PANI@ZnO/Fe_3O_4 nanocomposite

In pure PANI, three different phases of weight loss can be observed in the TGA profile (Fig. 8a). The weight loss in the first range up to 150 °C is mainly associated with evaporation of adsorbed moisture and volatile species, corresponding to a mass loss of about 4.2%. The second degradation phase, which takes place between 150 and 250 °C, is related to the loss of dopant species and partial decomposition of the conductive polymer backbone. resulting in a weight loss of about 13.8%. A major degradation stage occurs between approximately 250 and 400 °C with a mass loss of about 42.0%, indicating progressive breakdown of the molecular chains of PANI. A further degradation step between approximately 400 and 550 °C results in an additional weight loss of about 32.0%. Above 550 °C, the remaining carbonaceous residue gradually decomposes, leaving a final residue of approximately 8.0% at 800 °C. The modified degradation behavior of the hybrid nanocomposites is consistent with the incorporation of thermally stable inorganic ZnO and Fe_3O_4 phases into the PANI matrix. The DTG curve shown in Figure 8(b) contains thermal peaks at approximately 90 °C, 200 °C, 390 °C, and 520/°C. The peak at 90/°C corresponds to moisture evaporation, whereas the dominant degradation peak centered at 390 °C confirms the major thermal decomposition of PANI chains and degradation of the conjugated polymer structure. The peak at 520 °C is associated with the decomposition of residual carbonaceous fragments.

The TGA curve of the PANI@ZnO/Fe_3O_4 hybrid nanocomposite showed multiple thermal degradation steps related to moisture removal and polymer degradation, as shown in Fig. 8(c). The slight weight loss below approximately 200 °C corresponds to a mass loss of about 2.3%, resulting from evaporation of physically adsorbed moisture. The second degradation stage occurring up to approximately 320 °C exhibits a weight loss of about 8.6%, associated with the removal of volatile components and partial degradation of the conducting PANI backbone. The third degradation region between approximately 320 and 500 °C shows a weight loss of about 18.9%, while a further degradation stage between approximately 500 and 600 °C contributes an additional mass loss of about 30.2%. Above 600 °C, the residual mass remains comparatively stable due to the presence of thermally stable ZnO and Fe_3O_4 nanoparticles, resulting in a final residue of approximately 40.0% at 800 °C.

Figure 8(d) of the DTG profile shows thermal transitions at approximately 95 °C, 210 °C, 435 °C, and 590 °C, corresponding to moisture evaporation, dopant removal, polymer chain degradation, and decomposition of residual organic constituents, respectively. The major degradation peak centered at 435/°C indicates that the incorporation of ZnO and Fe_3O_4 nanoparticles shifts the decomposition temperature to a higher value compared with pure PANI, confirming the enhanced thermal stability of the hybrid nanocomposite system. Earlier studies revealed that, the nanocomposite exhibited a slower weight-loss rate and higher decomposition temperature, confirming the effectiveness of ZnO reinforcement in improving thermal durability. These results indicate that the PANI–ZnO nanocomposite is suitable for applications requiring enhanced thermal stability under elevated operating conditions (Handore *et al.* 2025).

3.5 Gas Sensing Studies

Ambient temperature gas sensing measurements were made using a custom-designed static gas detecting chamber as shown in Fig. 9. The sensors fabricated by the engineered PANI@ZnO/Fe_3O_4 hybrid nanocomposite were then introduced into the chamber, and the required amount of target gas was fed into the chamber using the calibrated syringe till the required concentration in parts per million (ppm) was reached. The sensing response was consistently measured until a stable value of the resistance was obtained. The recovery qualities of the sensor were assessed by subjecting the sensing element to fresh ambient air. Throughout the recovery procedure, both the input and outlet valves of the chamber were concurrently opened while a vacuum pump was activated to expedite gas extraction and chamber degassing. The inlet valve allowed for gas introduction, while the outlet valve allowed for efficient gas outflow from the detecting chamber.

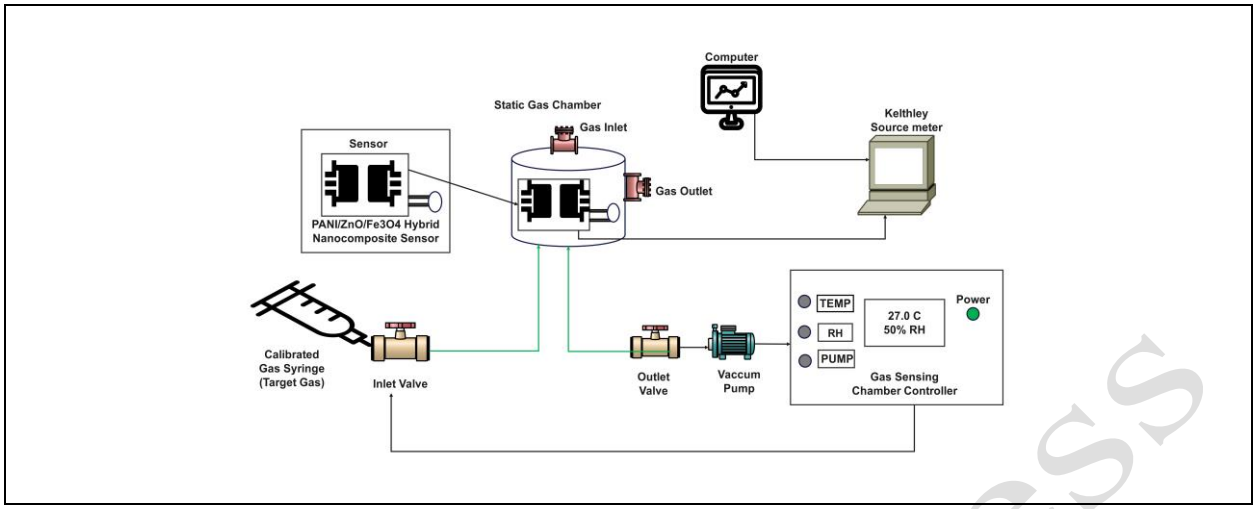

Fig. 9: Gas sensing experimental setup

The necessary gas concentration was achieved by the static gas distribution technique as specified in formula (Ullah *et al.* 2020).

$$C(\text{ppm}) = \frac{22.4\rho TV'}{273MV} \times 1000 \quad \ldots (4)$$

In the gas concentration equation, ρ (g mL^{-1}) indicates the density of the test gas, C (ppm) signifies target gas concentration, V_0 pertains to the injected gas volume, T represents the absolute temperature in Kelvin, M denotes the molecular mass of the gas, and V refers to effective volume of the sensing chamber in liters. In sensing studies, relative humidity and ambient temperature within the chamber were sustained at roughly 50% and 27 °C, respectively. The sensing efficacy of the constructed PANI@ZnO/Fe_3O_4 hybrid nanocomposite sensor was later assessed under these regulated environmental conditions:

$$R\% = \frac{R_a - R_g}{R_g} \times 100 \quad \ldots (5)$$

In the sensing measurements, R_a signifies the electrical resistance of the sensor in ambient air, whereas Rg indicates resistance when exposed to the target gas. The sensing qualities were additionally assessed by analysis of recovery times and response. The reaction time refers to the interval needed for the sensor to reach 90% of the complete resistance change following exposure to ammonia gas, whereas recovery time denotes the duration required for the sensor to restore 90% of its initial resistance value after the target gas was removed. The synthesized PANI@ZnO/Fe_3O_4 hybrid nanocomposite sensor demonstrated a concentration-dependent response to NH_3, exhibiting distinct response and recovery characteristics based on varied nanoparticle loadings and ammonia concentrations. The sensor's sensitivity was ascertained from the slope of the calibration curve established between the sensing response and the target gas concentration.

$$S = \Delta R/\Delta C \quad \ldots (6)$$

In this context, ΔR and ΔC represent variations in concentration and sensor response, respectively.

3.5.1 Sensor Response and Sensitivity Analysis

The sensing capabilities for NH_3 gas were significantly affected by the recovery and response characteristics of the PANI@ZnO/Fe_3O_4 hybrid nanocomposite sensor at varying nanoparticle concentrations. Figure 10 depicts the NH_3 sensing efficacy across a concentration range of 50–300 ppm, as indicated by fluctuations in sensor resistance. The resistance of both PANI and PANI@ZnO/Fe_3O_4 hybrid nanocomposite films increased significantly with rising NH_3 concentration, as illustrated in Fig. 10(a), signifying improved charge transfer interactions between ammonia molecules and the conductive sensing layer.

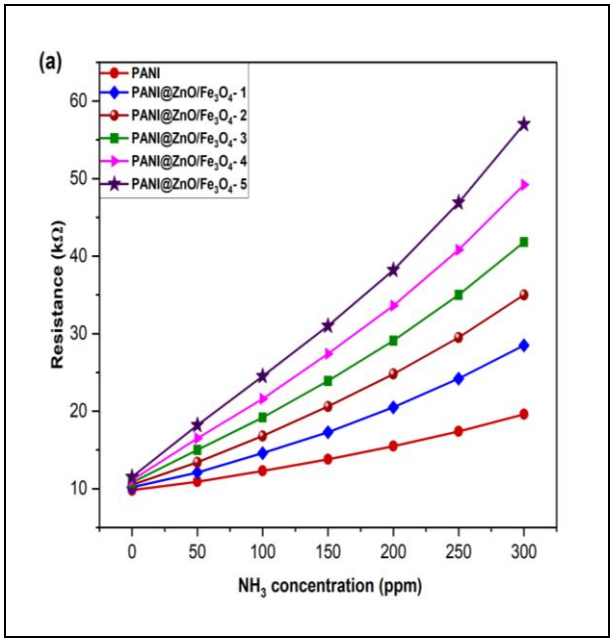

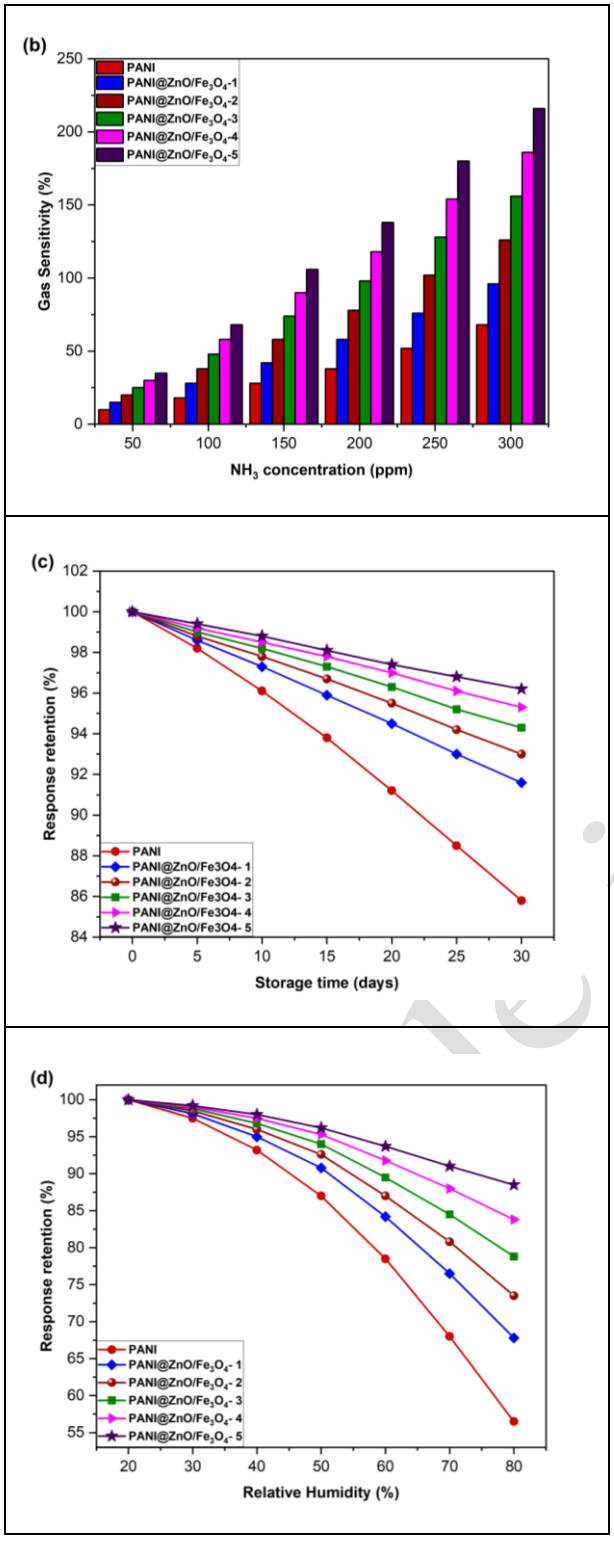

Fig. 10: (a) Resistance response of sensors toward NH_3 gas, (b) Gas sensing sensitivity of prepared films, (c) Long-term stability of hybrid nanocomposite sensors and (d) Influence of humidity on ammonia sensing behavior

Upon exposure to NH_3 concentrations ranging from 50 to 300 ppm, the resistance fluctuations of the constructed sensors were as follows: 11.8–28.6 kΩ for PANI@ZnO/Fe_3O_4-1, 13.1–35.0 kΩ for PANI@ZnO/Fe_3O_4-2, 14.7–41.8 kΩ for PANI@ZnO/Fe_3O_4-3, 16.2–49.2 kΩ for PANI@ZnO/Fe_3O_4-4, 18.1–56.8 kΩ for PANI@ZnO/Fe_3O_4-5, and 10.8–19.5 kΩ for pure PANI sensors. The progressive increase in NH_3 response with ZnO/Fe_3O_4 loading demonstrates a clear composition-dependent sensing behavior, with PANI@ZnO/Fe_3O_4-5 exhibiting the highest response within the investigated range. This improvement may be associated with changes in the physicochemical environment of the PANI matrix following nanoparticle incorporation; however, the precise interfacial sensing mechanism requires further direct investigation.

Figure 10(b) depicts the sensing response relative to NH_3 concentration for the assessment of sensor sensitivity. The sensing response values increased from approximately 10–125% for pure PANI, 15–95% for PANI@ZnO/Fe_3O_4-1, 20–125% for PANI@ZnO/Fe_3O_4-2, 24–155% for PANI@ZnO/Fe_3O_4-3, 29–185% for PANI@ZnO/Fe_3O_4-4, and 34–215% for PANI@ZnO/Fe_3O_4-5 as the NH_3 concentration increased from 50 to 300 ppm. Linear regression of the calibration response for the PANI@ZnO/Fe_3O_4-5 sensor over the investigated NH_3 concentration range of 50–300 ppm yielded a sensitivity of 0.727 % ppm^{-1} with a coefficient of determination (R^2) of 0.9989, indicating a strong linear concentration-dependent sensing response.

Figure 10(c) shows the sensing stability of pure PANI and PANI@ZnO/Fe_3O_4-1–5 hybrid nanocomposite sensors toward NH_3 gas for 30 days and demonstrates reliable sensing performance over the testing period. The response retention after 30 days was approximately 85.8% for pure PANI, 91.6% for PANI@ZnO/Fe_3O_4-1, 93.0% for PANI@ZnO/Fe_3O_4-2, 94.4% for PANI@ZnO/Fe_3O_4-3, 95.3% for PANI@ZnO/Fe_3O_4-4, and 96.2% for PANI@ZnO/Fe_3O_4-5.

The sensing efficiency of PANI and PANI@ZnO/Fe_3O_4 hybrid nanocomposite films was evaluated for 100 ppm NH_3 exposure at different relative humidity levels.

The sensing response of PANI and PANI@ZnO/Fe_3O_4 hybrid nanocomposite sensors as a function of relative humidity is shown in Figure 10(d). The best sensing ability of the sensor was obtained at 20% RH, where all sensors exhibited nearly 100% response retention. The response retention at 80% RH was approximately 56.5% for pure PANI, 67.8% for PANI@ZnO/Fe_3O_4-1, 73.4% for PANI@ZnO/Fe_3O_4-2, 78.8% for PANI@ZnO/Fe_3O_4-3, 83.7% for PANI@ZnO/Fe_3O_4-4, and 88.5% for PANI@ZnO/Fe_3O_4-5, demonstrating the superior humidity tolerance of the hybrid nanocomposite sensors. Prior research demonstrates that the PANI-Fe_2O_3 nanocomposites were synthesized by electrochemical polymerization with

varying Fe_2O_3 concentrations to examine their structural, dielectric, and optical properties. The study found that Fe_2O_3 incorporation enhanced light absorption and manipulated nonlinear optical properties, while PANI showed a high specific capacitance of 477 F g^{-1}, positioning these materials as strong candidates for optoelectronics and energy storage applications (Al-Gharram and AlZoubi, 2025).

3.5.2 Sensor Response and Recovery Behavior

Figure 11 depicts recovery time (T_2) and response time (T_1) attributes of pure PANI and PANI@ZnO/Fe_3O_4 hybrid nanocomposite sensors at varying NH_3 gas concentrations. The differences in response and recovery behavior illustrate the impact of including ZnO and Fe_3O_4 nanoparticles on the adsorption-desorption kinetics and charge transfer efficiency of sensing material then exposed to ammonia.

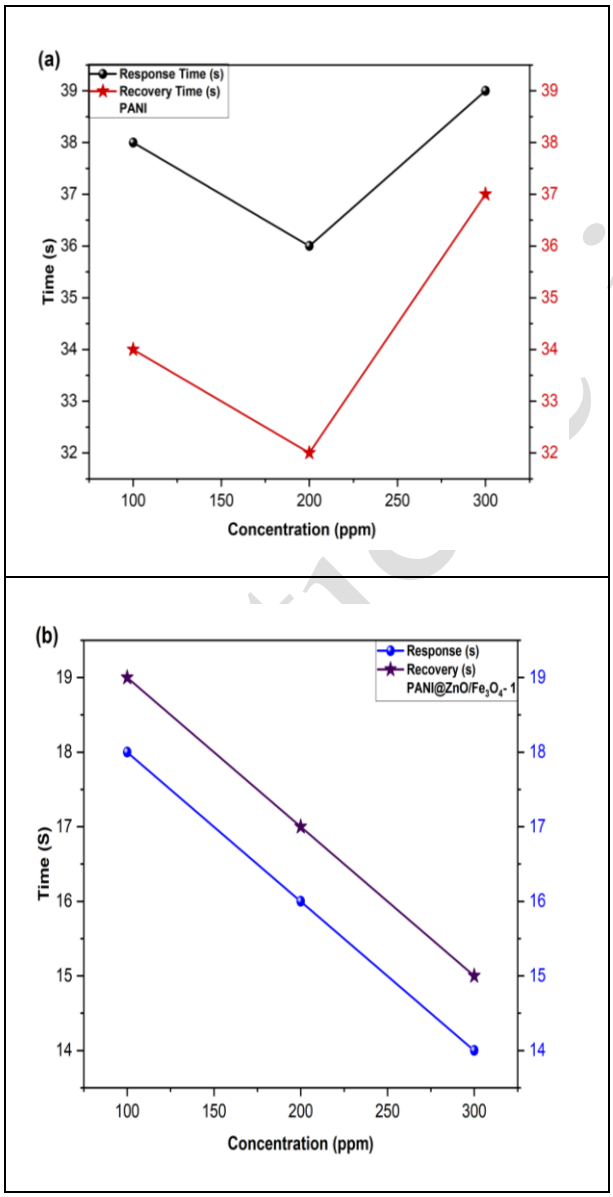

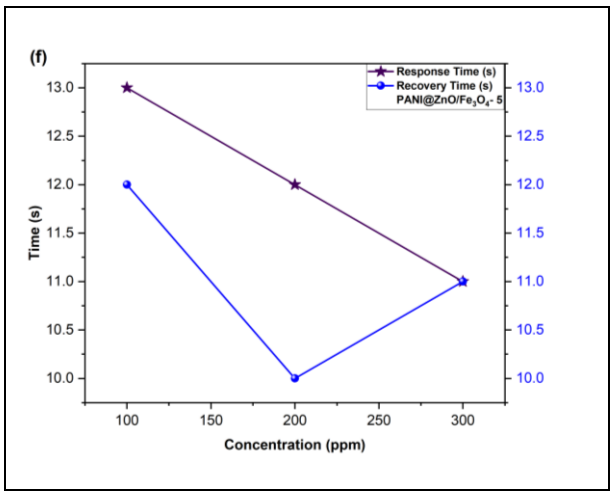

Fig. 11: (a) Response–recovery curves of PANI gas sensor (b) - (f) Response–recovery curves of PANI@ZnO/Fe_3O_4 sensors

The response time of pure PANI varied from 38 s at 100 ppm, 36 s at 200 ppm, and 39 s at 300 ppm, while the corresponding recovery times were 34 s, 32 s, and 37 s, respectively, as NH_3 concentration increased from 100 ppm to 300 ppm.

On the other hand, the hybrid nanocomposite sensors had demonstrated significantly shorter sensing parameters; of which PANI@ZnO/Fe_3O_4-1 sample had shorter response and recovery times of 18 s and 19 s at 100 ppm, 16 s and 17 s at 200 ppm, and 14 s and 15 s at 300 ppm, respectively. The PANI@ZnO/Fe_3O_4-2 sample showed response and recovery times of 16 s and 14 s at 100 ppm, 14 s and 12 s at 200 ppm, and 12 s and 11 s at 300 ppm, respectively. Similarly, the PANI@ZnO/Fe_3O_4-3 sample exhibited response times of 15 s, 13 s, and 11 s with corresponding recovery times of 13 s, 11 s, and 12 s at 100, 200, and 300 ppm, respectively. The PANI@ZnO/Fe_3O_4-4 sample showed response times of 16 s, 15 s, and 14 s, whereas the recovery times were 14 s, 12 s, and 13 s, respectively. The PANI@ZnO/Fe_3O_4-5 sample demonstrated response times of 13 s, 12 s, and 11 s, with recovery times of 12 s, 10 s, and 11 s at 100, 200, and 300 ppm, respectively.

The hybrid nanocomposite PANI@ZnO/Fe_3O_4-5 at 300 ppm NH_3 exhibited the lowest response time of approximately 11 s and a recovery time of approximately 11 s, indicating the fastest sensing performance among all the fabricated sensors. The improved response and recovery behavior of the PANI@ZnO/Fe_3O_4 hybrid nanocomposites may be associated with the combined influence of PANI, ZnO, and Fe_3O_4 on the physicochemical environment of the sensing layer. The incorporation of ZnO and Fe_3O_4 may modify the interfacial environment and NH_3 adsorption characteristics, thereby contributing to the observed resistance changes. However, in the absence of direct surface and electrical characterization such as XPS and impedance spectroscopy, the specific interfacial charge-transfer processes cannot be conclusively established. Previous studies report that ZnO-PANI nanocomposites electrodeposited on a glassy carbon electrode, further modified with laccase enzymes and polypyrrole, were used to fabricate a biosensor for detecting the cationic surfactant CTAB. The sensor showed high sensitivity of 0.935 $\mu A \mu M^{-1} cm^{-2}$, an exceptionally low detection limit of 0.0116 µM, and reliable recovery rates in both tap water and wastewater samples (Kyomuhimbo *et al.* 2024).

3.5.3 Selectivity Performance of PANI@ZnO/Fe_3O_4 Sensor

Selectivity performance of pure PANI and PANI@ZnO/Fe_3O_4 hybrid nanocomposite films was rigorously assessed with the inclusion of various interfering gases. Figure 12 demonstrates the sensing responses of PANI and PANI@ZnO/Fe_3O_4 hybrid sensors that were exposed to 100 ppm concentrations of NH_3, hydrogen sulfide (H_2S), carbon monoxide (CO), carbon dioxide (CO_2), and ethanol (C_2H_5OH), aimed at assessing their gas discrimination capability and selective ammonia sensing behavior.

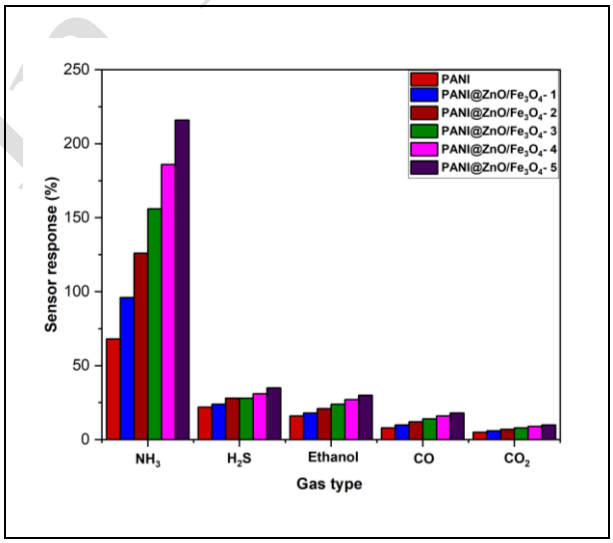

Fig. 12: Gas selectivity performance of PANI nanocomposites

In comparison to other evaluated gases, the PANI@ZnO/Fe_3O_4 hybrid nanocomposite sensor demonstrated a markedly enhanced response to NH_3 gas. The sensor response toward NH_3 increased progressively from approximately 68% for pure PANI to 95%, 125%, 155%, 185%, and 215% for PANI@ZnO/Fe_3O_4-1, PANI@ZnO/Fe_3O_4-2, PANI@ZnO/Fe_3O_4-3, PANI@ZnO/Fe_3O_4-4, and PANI@ZnO/Fe_3O_4-5, respectively. For H_2S gas, the sensor responses were approximately 20%, 22%, 25%, 27%, 30%, and 34%, whereas for ethanol they were 15%, 18%, 20%, 23%, 26%, and 29% for pure PANI through PANI@ZnO/Fe_3O_4-5, respectively. Similarly, the

responses toward CO were limited to approximately 6%, 8%, 10%, 12%, 14%, and 16%, while the responses toward CO_2 remained very low at approximately 4%, 5%, 6%, 7%, 8%, and 9%, respectively.

Ammonia molecules exhibit significant polarity and reactive lone-pair electrons, which interact robustly with the conductive PANI backbone via charge transfer and protonation–deprotonation pathways. The addition of ZnO and Fe_3O_4 nanoparticles significantly improved the sensing performance by augmenting the quantity of active adsorption sites and enhancing catalytic activity within the hybrid nanocomposite matrix. The acidic properties of PANI enhanced interaction with basic NH_3 molecules, leading to significant alterations in electrical conductivity and sensor resistance. In contrast, gases like carbon monoxide, hydrogen sulfide, carbon dioxide, and ethanol demonstrated weaker interactions with the sensing surface due to their diminished adsorption affinity and restricted charge transfer capacity. The higher NH_3 selectivity of the PANI@ZnO/Fe_3O_4 hybrid nanocomposite sensor was primarily due to improved adsorption kinetics, effective electron transfer, and synergistic catalytic interactions among PANI, ZnO, and Fe_3O_4 nanoparticles.

3.5.4 Gas Sensing Mechanism of PANI@ZnO/Fe_3O_4

The NH_3 sensing mechanism of the PANI@ZnO/Fe_3O_4 hybrid nanocomposite was primarily influenced by changes in electrical conductivity due to interactions between ammonia molecules and the conductive sensor surface. PANI functions as a conducting polymer matrix, and when exposed to NH_3 gas, charge transfer interactions transpire due to the basic characteristics of ammonia and the presence of lone-pair electrons on the nitrogen atom, as depicted in Fig. 13(a).

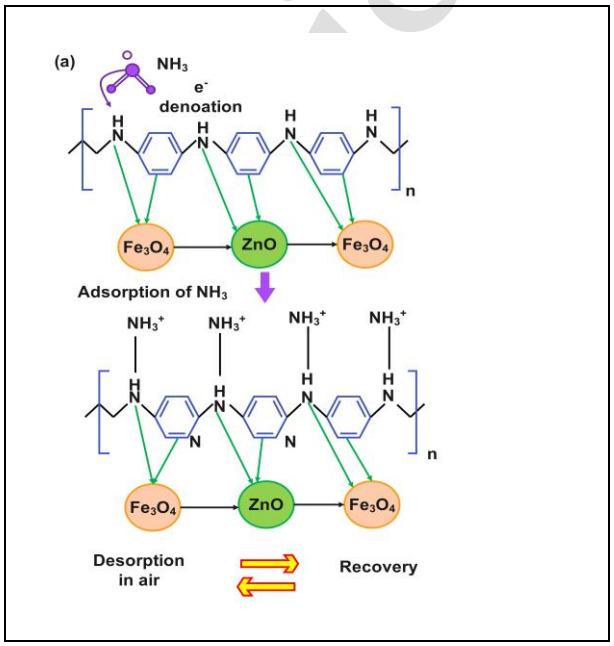

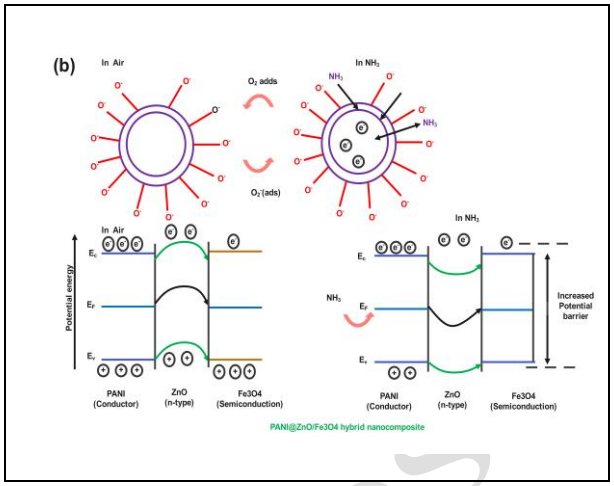

Fig. 13: (a) Schematic ammonia sensing mechanism of PANI@ZnO/Fe_3O_4 and (b) Band structure of hybrid nanocomposite under NH_3 exposure

When NH_3 molecules interact with the conductive PANI matrix, they gain electrons, and the number of hole charge carriers in the matrix decreases, causing the electrical conductivity of the sensing material to decrease. Incorporating both ZnO and Fe_3O_4 nanoparticles enhances the sensing process by providing additional active adsorption sites and catalyzing interactions between the ammonia molecules. The synergistic integration of conductive PANI with semiconducting ZnO and Fe_3O_4 nanoparticles favors the charge transfer efficiency and the rapid electron exchange with NH_3 exposure, resulting in a significant change in the electrical resistance. Furthermore, the hybrid nanostructure changes the electronic band alignment by forming localized energy states within the PANI matrix that further enhance the gas adsorption and carrier transport properties. This adsorption of NH_3 causes electrons to be donated from the ammonia, altering the Fermi level and the conduction channel of the nanocomposite, and thus its charge transport properties, and therefore the sensing layer. The heterojunction network between PANI, ZnO, and Fe_3O_4 nanoparticles is found to be effective in modulating the sensitivity and selectivity of the metal oxide nanoparticles and the conductivity of the heterojunction network upon exposure to ammonia gas. In this way, the energy barrier for carrier mobility increases upon the adsorption of NH_3 molecules and, consequently, the function of the sensor to PANI@ZnO/Fe_3O_4hybrid nanocomposite is quantifiable resistance change, which is observed upon the adsorption of NH_3 molecules.

4. CONCLUSION

PANI@ZnO/Fe_3O_4 hybrid nanocomposites were successfully synthesized through chemical oxidative polymerization and evaluated for room-temperature NH_3 sensing. The incorporation of ZnO and Fe_3O_4 modified the structural, optical, and thermal

characteristics of PANI, with the optical band gap progressively decreasing from 3.18 to 2.79 eV. Among the fabricated sensors, PANI@ZnO/Fe_3O_4-5 exhibited the highest response of approximately 215% toward 300 ppm NH_3, with response and recovery times of approximately 11 s. The sensor also showed preferential response toward NH_3 over the tested interfering gases and retained 96.2% of its initial response after 30 days. The study demonstrates that controlled incorporation of ZnO and Fe_3O_4 provides an effective strategy for tuning the physicochemical characteristics and room-temperature NH_3 sensing performance of PANI-based hybrid materials. These findings contribute to the development of conductive-polymer/metal-oxide hybrid platforms for ambient gas sensing. Nevertheless, the present investigation was limited to controlled laboratory conditions and a restricted range of interfering gases. Future studies should address lower NH_3 concentrations, extended operational durability, complex gas mixtures, real-world environmental conditions, and practical device integration.

FUNDING

This research received no specific grant from any funding agency in the public, commercial, or not-for-profit sectors.

CONFLICTS OF INTEREST

The authors declare that there is no conflict of interest.

COPYRIGHT

REFERENCES

Al-Gharram, M. and AlZoubi, T., Exploring dual optical responses of Polyaniline-Fe_2O_3 nanocomposites for advanced optoelectronic and supercapacitor applications, *Ceram. Int.*, 51(18), 24916–24934 (2025). https://doi.org/10.1016/j.ceramint.2025.03.173

Al-Gharram, M., Uhlmann, P. and Al-Hussein, M., Highly dispersed crystalline magnetic and conductive polyaniline/iron oxide nanocomposite films, *Colloids Surf. A: Physicochem. Eng. Aspects*, 684, 133212(2024). https://doi.org/10.1016/j.colsurfa.2024.133212

Andre, R. S., Dos Santos, D. M., Mercante, L. A., Facure, M. H. M., Campana-Filho, S. P., Mattoso, L. H. C. and Correa, D. S., Nanochitin-based composite films as a disposable ethanol sensor, *J. Environ. Chem. Eng.*, 8(5), 104163(2020). https://doi.org/10.1016/j.jece.2020.104163

Basha, B., Aldhafeeri, T. R., Tariq, R., Akhtar, M., Alsaiari, N. S., Al-Buriahi, M. S., Warsi, M. F. and Zulfiqar, S., Carbonaceous glass electrode fabricated with L-cysteine incorporated C@Fe_2O_3 for the ultra-selective determination of toxic metal ions, *J. Water Process Eng.*, 75, 107897(2025). https://doi.org/10.1016/j.jwpe.2025.107897

Bilgic, A. and Cimen, A., A highly sensitive and selective ON-OFF fluorescent sensor based on functionalized magnetite nanoparticles for detection of Cr(VI) metal ions in the aqueous medium, *J. Mol. Liq.*, 312, 113398(2020). https://doi.org/10.1016/j.molliq.2020.113398

Buledi, J. A., Shaikh, H., Solangi, A. R., Mallah, A., Shah, Z. U. H., Khan, M. M., Sanati, A. L., Karimi-Maleh, H., Karaman, C., Camarada, M. B. and Niculina, D. E., Synthesis of NiO-Doped ZnO Nanoparticle-Decorated Reduced Graphene Oxide Nanohybrid for Highly Sensitive and Selective Electrochemical Sensing of Bisphenol A in Aqueous Samples, *Indus. Eng. Chem. Res.*, 62(11), 4754–4764 (2023). https://doi.org/10.1021/acs.iecr.2c04091

Daramola, O. B., Torimiro, N., George, R. C., Daramola, I. V and Omole, R. K., Affinity Capture Using Ligand and Polymer-Functionalized Iron Oxide, Gold and Iron-Gold Nanocomposites to Target Enteric Bacteria, *BioNanoSci.*, 15(1), 8(2025). https://doi.org/10.1007/s12668-024-01682-9

Manasa, G., Mascarenhas, R. J. and Basavaraja, B. M., Sensitively-selective determination of Propyl Paraben preservative based on synergistic effects of polyaniline-zinc-oxide nano-composite incorporated into graphite paste electrode, *Colloids Surf. B: Biointerf.*, 184, 110529(2019). https://doi.org/10.1016/j.colsurfb.2019.110529

Ghaffarirad, M. A., Sabahi, A., Golshani, Z., Manteghi, F. and Ghaffarinejad, A., Non-enzymatic glucose electrochemical sensor based on nitrogen-doped graphene modified with polyaniline and Fe_3O_4@MIL-101-NH_2 nano framework, *Inorg. Chem. Commun.*, 159, 111812(2024). https://doi.org/10.1016/j.inoche.2023.111812

Gunasekaran, Y., Suntharam, N. M., Bashir, S., Vengadaesvaran, B., Gunasegeran, S., Gopalakrishnan, N., Ramesh, S., Ramesh, K., Gerard, O. and Pershaanaa, M., Synthesis and characterization of ZnO/biochar composite as electrode material for hybrid supercapacitor, *Ionics*, 32(2), 1987-2010(2025). https://doi.org/10.1007/s11581-025-06839-4

Handore, K. N., Sharma, S. B. and Chabukswar, V. V., One-pot ultrasound synthesis of polyaniline–ZnO and its synergistic effect on microbial activity, *RSC Adv.*,

15(45), 37856–37864(2025). https://doi.org/10.1039/d5ra04461h

Hasan, I. M. A., Tawfik, A. R. and Assaf, F. H., Green Iron Oxide Nanoparticles as a Modifier of Carbon Paste Electrode for Electrochemical Estimation of Paracetamol in Pharmaceutical Samples, *Russian J. Electrochem.*, 57(5), 435–447 (2021). https://doi.org/10.1134/s1023193521050050

Kyomuhimbo, H. D., Feleni, U., Haneklaus, N. H. and Brink, H. G., ZnO–Polyaniline Nanocomposite Functionalised with Laccase Enzymes for Electrochemical Detection of Cetyltrimethylammonuium Bromide (CTAB), *J. Xenobio.*, 14(4), 1988–2002 (2024). https://doi.org/10.3390/jox14040106

Liu, X., Gao, T., Liu, H., Fang, Y. and Wang, L., Fabrication of peroxidase-mimic iron oxide/carbon nanocomposite for highly sensitive colorimetric detection, *J. Exp. Nanosci.*, 17(1), 75–85 (2022). https://doi.org/10.1080/17458080.2022.2030470

Mahmood, W. K., Rashid, T. M., Rahmah, M. I., Jasim, A. M., Fahem, M. Q., Jabir, M. S., Abid, D. A., Majed, R. A., Awaid, D. M. and Yosif, H. M., Empowering NO_2 Detection: Synthesis of Highly Responsive Au/Cu-Doped Iron Oxide Nanoparticles as Gas Sensors Through Laser Ablation, *Plasmonics*, 19(6), 3167–3176 (2024). https://doi.org/10.1007/s11468-024-02235-2

Murugan, S., Srinivasan, G., Kotteeswaran, S., Jeyaraj, W., Govindasamy, M. and Thangavel, K., Green synthesis of Ag_2O/ZnO nanocomposite for efficient antibacterial property and tunable electrochemical detection of hydrogen peroxide, *J. Environ. Chem. Eng.*, 13(3), 116394(2025). https://doi.org/10.1016/j.jece.2025.116394

Murugesan, K., Das, S. and Dutta, K., Application of polyaniline/zinc oxide nanocomposites for non-enzymatic cholesterol detection: A preliminary investigation on the effect of dopants on the morphology, thermal stability, electrochemical and sensing behavior of the nanocomposites, *Polym. Plast. Technol. Mater.*, 63(10), 1239–1253 (2024). https://doi.org/10.1080/25740881.2024.2326144

Mutlaq, S., Albiss, B., Al-Nabulsi, A. A., Jaradat, Z. W., Olaimat, A. N., Khalifeh, M. S., Osaili, T., Ayyash, M. M. and Holley, R. A., Conductometric immunosensor for escherichia coli o157:H7 detection based on polyaniline/zinc oxide (pani/zno) nanocomposite, *Polym.*, 13(19), 3288(2021). https://doi.org/10.3390/polym13193288

Niaz, A., Arain, M. B. and Soylak, M., Simultaneous voltammetric determination of dopamine and uric acid using screen printed carbon electrode modified with quercetin functionalized-iron oxide nanoparticles, *Mater. Res. Bull.*, 185, 113317(2025). https://doi.org/10.1016/j.materresbull.2025.113317

Pakapongpan, S., Poo-arporn, Y., Tuantranont, A. and Poo-arporn, R. P., A facile one-pot synthesis of magnetic iron oxide nanoparticles embed N-doped graphene modified magnetic screen printed electrode for electrochemical sensing of chloramphenicol and diethylstilbestrol, *Talanta*, 241, 123184(2022). https://doi.org/10.1016/j.talanta.2021.123184

Pandey, A., Saini, S. K., Singh, R. K. and Mohanty, T., Power dependent tunable optical nonlinearity in Iron oxide/Borophene core-shell nanoparticles under ultrashort laser excitation, *Optics Laser Technol.*, 181, 111761(2025). https://doi.org/10.1016/j.optlastec.2024.111761

Rajyashree, L., Manoharan, C., Loganathan, A. and Venkateshwarlu, M., Electrochemical and sensing properties of α-Fe_2O_3 nanoparticles synthesized using hydrothermal method at low reaction temperature, *J. Mater. Sci. Mater. Electron.*, 34(6), 462(2023). https://doi.org/10.1007/s10854-023-09822-9

Shanavash, A., Sri, T. S., Mayakannan, S., Shanmugam, S. K., Chandankhede, P. H. and Sivakumar, B. G., Development of a carbon–perovskite self-powered IoT sensor node with dual-mode sensing, *Interact.*, 247(1), 175(2026). https://doi.org/10.1007/s10751-026-02516-8

Singh, V. P., Singh, C. P., Kumar, S., Pandey, S. K. and Punetha, D., Microwave-Assisted Synthesis and Characterization of Iron Oxide Nanoparticles for Advanced Biomedical Sensing Applications, *IEEE Open J. Nanotechnol.*, 6, 10–15(2025). https://doi.org/10.1109/OJNANO.2024.3514866

Tamilarasi, K., Jayasurrya, M., Meena, M., Vimalan, M. and Vetha, P. I., Novel PANI–Pb_3O_4 composites with enhanced electrochemical properties for supercapacitor application, *J. Mater. Sci. Mater. Electron.*, 37(14), 1038(2026). https://doi.org/10.1007/s10854-026-17397-4

Toderascu, L. I., Sima, L. E., Orobeti, S., Florian, P. E., Icriverzi, M., Maraloiu, V.-A., Comanescu, C., Iacob, N., Kuncser, V., Antohe, I., Popescu-Pelin, G., Stanciu, G., Ionita, P., Mihailescu, C. N. and Socol, G., Synthesis and Anti-Melanoma Activity of L-Cysteine-Coated Iron Oxide Nanoparticles Loaded with Doxorubicin, *Nanomater.*, 13(4), 621(2023). https://doi.org/10.3390/nano13040621

Tümay, S. O., Şanko, V., Şenocak, A. and Demirbas, E., A hybrid nanosensor based on novel fluorescent iron oxide nanoparticles for highly selective determination of Hg_2^+ions in environmental samples, *New J. Chem.*, 45(32), 14495–14507 (2021). https://doi.org/10.1039/d1nj02908h

Ullah, N., Ali Shah, A. U. H., Jan, F. A., Ansir, R. and Muhammad, W., Application of modified PANI-ZnO composites for NH_3Gas sensor at ambient temperature, *J. Chem. Soc. Pakistan*, 42(3), 390–398 (2020).

Velayudham, R. and Natarajan, J., Multifunctional application of different iron oxide nanoparticles, *Zeitschrift Fur Physikalische Chemie*, 239(2–3), 379–395 (2025). https://doi.org/10.1515/zpch-2024-0745

Yan, S., Shen, D., Xin, B., Newton, M. A. A. and Wu, Y., Rhombus-patterned flexible self-supported PVDF-based humidity sensor for respiratory monitoring, *Polym.*, 282, 126139(2023). https://doi.org/10.1016/j.polymer.2023.126139

Yang, J., Du, M., Wu, W., Chen, Q., Niu, J. and Zhang, Z., Polyaniline-modified iron oxide nanoparticles to improve the overall performance of MFC-BOD sensors, *J. Water Process Eng.*, 71, 107189(2025). https://doi.org/10.1016/j.jwpe.2025.107189

Yang, Q., Li, N., Li, Q., Chen, S., Wang, H. L. and Yang, H., Amperometric sarcosine biosensor based on hollow magnetic Pt–Fe_3O_4@C nanospheres, *Anal. Chimica Acta*, 1078, 161–167 (2019). https://doi.org/10.1016/j.aca.2019.06.031

Yang, Z., Liu, Q., Zhang, L., Dai, J. and Shen, Z., Green one-pot synthesis of binder-free porous edge-functionalized graphitic carbon nitride/iron oxide nanoparticles nanocomposite as an outstanding electrode for supercapacitors, *J. Energy Storage*, 32, 101909 (2020). https://doi.org/10.1016/j.est.2020.101909

Yıldız, D. E., Unal, F. and Taşaltın, N., Non-enzymatic electrochemical voltammetric sensors based on thulium:zinc oxide for dopamine detection, *J. Mater. Sci. Mater. Electron.*, 35(7), 475(2024). https://doi.org/10.1007/s10854-024-12155-w